Analysis of Picosecond Pulse Shape Synthesis by Spectral Masking in a Grating Pulse Compressor

ROBERT N. THURSTON, JONATHAN P. HERITAGE, ANDREW M. WEINER, AND W. J. TOMLINSON

Abstract—**This paper analyzes the synthesis of arbitrarily shaped optical pulses by spectral filtering in a fiber-and-grating pulse compressor. Spectral filtering of phase and amplitude is achieved by masking the spatially dispersed frequency components within the compressor. We show that the spectral filter is the convolution of the mask with the beam's transverse intensity profile. We discuss the effect of diffraction from the features of the physical mask, and show how finite spatial resolution limits the range of attainable temporal profiles. The fundamental limitation on spectral resolution is derived. Spectra and temporal pulse shapes corresponding to a variety of physical masks are calculated and are found to be in excellent agreement with experiments done with compressed pulses from a mode-locked Nd:YAG laser.**

Introduction

We have previously demonstrated a technique for synthesizing arbitrary optical pulse shapes by filtering the spatially dispersed Fourier components in a fiber-and-grating pulse compressor [1]. We produced a variety of picosecond pulse shapes by introducing simple geometrical amplitude and phase filters at the appropriate location in the pulse compressor. The ability to arbitrarily shape picosecond and subpicosecond optical pulses will have important applications in optical communications and optical radar as well as in picosecond and femtosecond spectroscopy. It is thus important to develop a computational model that will accurately predict the temporal pulse shapes that will be produced by the complicated masks that real applications will require.

The purpose of this paper is to develop and test this computational tool. This model is an extension of the approach of Tomlinson et al. [2] for calculating spectral broadening and pulse compression in a fiber-and-grating pulse compressor. We add to this calculational scheme an effective mask, or frequency filter, whose transfer function properly accounts for the influence of the physical mask which is inserted into the spatially dispersed beam within the compressor. We show that the effective mask is obtained by a convolution of the physical mask with the intensity profile of the beam. This procedure takes into account the influence of diffraction from the physical mask and of finite beam diameter; together, these effects determine the spectral resolution and thus impose limitations on the range of pulse shape features which may be synthesized. The finite beam diameter at the mask limits the width of a time window over which the temporal profile of a single pulse can be effectively tailored. Effects due to diffraction from sharp boundaries in the physical mask present an especially stringent test of the theory since sharp features in the frequency domain are evident as readily observed broad features in the time domain. We have calculated spectra and autocorrelation shapes for a variety of physical masks, including masks with sharp boundaries, and without adjusting any parameters, we find excellent agreement with pulse-shaping experiments done with compressed pulses from a mode-locked Nd:YAG laser [1], [3], [4]. The pulse shapes considered include bursts of evenly spaced pulses, a pulse doublet with odd field symmetry, a square pulse, and a pair of square pulses. Our results show that the model may be used with confidence to predict the pulse shapes for more complicated physical masks.

Manuscript received October 22, 1985; revised January 22, 1986.

The authors are with Bell Communications Research, Navesink Research and Engineering Center, Red Bank, NJ 07701-7020.

IEEE Log Number 8607767.

I. Overview

To model the effect of a mask, we start with a representation of a chirped pulse in the time domain, Fourier transform to the frequency domain, subtract from the phase a term quadratic in the frequency to simulate the action of the grating compressor, apply the mask, and then do the inverse Fourier transform to see the shaped and compressed pulse in the time domain. A general mask filters both amplitude and phase of the spectral components that are spatially spread by the grating.

In the experimental realization shown in Fig. 1, the frequency-modulated pulses emerging from a single-mode polarization-preserving fiber enter a double-pass folded-path grating compressor [3], [5]. The fiber chirps the pulses by self phase modulation and group velocity dispersion [2]. The grating pair does two things: it compresses the pulses by supplying the quadratic phase correction needed to compensate a linear frequency chirp, and it spreads (disperses) the spectrum spatially so that a physical mask can filter the frequencies. On the backward pass through the grating compressor, the phase correction continues while the spatial spreading of the spectrum is undone. As shown in Fig. 1, the masks are placed just after the first pass through the grating pair where the spectrum is maximally spread in space. Each pulse goes through the mask twice.

The spatial dispersion of the spectrum maps the frequency coordinate onto the spatial coordinate x on the mask. With perfect resolution, the effective filter function

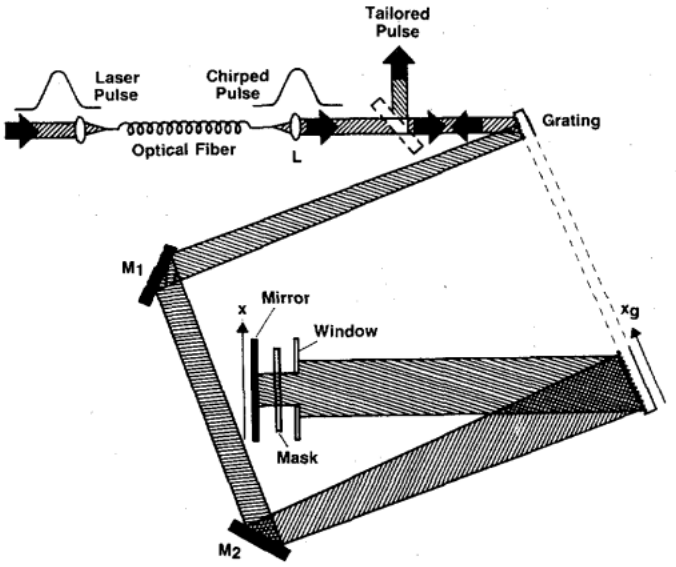

Fig. 1. Experimental setup. The optical fiber chirps the laser pulse, primarily by self phase modulation. There is also a contribution from group velocity dispersion. The single grating is equivalent to a pair of parallel gratings because of the path folding by the mirrors M_1 and M_2. The grating applies the quadratic phase correction needed to compress a linearly chirped pulse, and it produces the spatial dispersion of the spectrum that allows a mask to filter the frequencies. The resolution is limited by the spot size at the mask. The axes x and x_g are used in the derivation of (2.4).

in the frequency domain would be simply the mask transmission function $M(x)$ with x replaced by the corresponding frequency. However, because each spectral component has a finite spot size w_0 at the mask, the effective filter function is smeared. Experimentally, this smearing is minimized by imaging the fiber output spot onto the turnaround mirror. Nevertheless, the finite spot size determines the spectral resolution and leads to diffraction from sharp boundaries in the physical mask. To obtain realistic results, the finite spot size and the energy lost by diffraction must be accounted for.

The preceding discussion implies that four essential inputs to the modeling calculation are 1) a realistic chirped input pulse, 2) the quadratic phase correction coefficient, 3) the spectral spreading parameter, and 4) the spot size w_0 at the mask. These items will be treated in detail in the remainder of the paper, in which we shall describe the analysis and compare calculated and experimental results. The calculations agree well with experiment, without adjustment of the parameters.

II. Fiber and Grating Compressor

A. Chirped Pulse (Effect of Fiber)

A good simulation of our pulse-shaping experiments depends on a good quantitative description of the chirped pulse which emerges from the optical fiber. At the experimental wavelength of 1064 nm and fiber length of 450 m, effects due to group velocity dispersion (GVD) and fiber loss are smaller than those due to self phase modulation (SPM). Calculations which include only SPM give results similar to those which include GVD and fiber loss as well. Nevertheless, we have simulated the chirped pulse in two different ways: 1) SPM only, and 2) integration of the nonlinear Schrödinger equation, which includes GVD and loss, as well as SPM. GVD affects the temporal width and shape of the pulse envelope, whereas SPM alone does not. In both cases, the inputs to the calculation can be adjusted to yield a simulated chirped pulse of the correct (experimentally measured) spectral width. (We take the spectral width as the primary experimentally determined parameter rather than peak intensity in the fiber because of experimental uncertainty in the latter.) Nonlinear pulse propagation in optical fibers has been adequately described in the literature [2], [6]–[9]. However, in order to document the results of this paper, we indicate the necessary details in Appendix A.

B. Grating Equations

1) Angular Dispersion: The angular dispersion of the grating allows a physical mask to filter the frequencies, and it is responsible for the quadratic phase correction that compresses the pulse. The angular dispersion in the first-order diffraction pattern reflected from the grating satisfies

$$\lambda = d(\sin\theta_i + \sin\theta_r), \tag{2.1}$$

from which

$$d\theta_r/d\lambda = 1/(d\cos\theta_r). \tag{2.2}$$

Here d is the spacing of the grating lines and θ_i and θ_r are the angles of incidence and refraction, both on the same side of the normal to the grating.

2) Spatial Dispersion: To calculate the spatial dispersion, let R be the path length between the first bounce off the grating where the essentially collimated incident light is angularly dispersed and the second bounce where it is again collimated. Then the wavelength-independent perpendicular distance between the gratings of the effective "grating pair" is $B = R\cos\theta_r$. (Because of the path folding by mirrors M_1 and M_2 in Fig. 1, the single grating in our setup functions as a pair of parallel gratings facing each other, separated by the perpendicular distance B.) The angularly dispersed light is brought to a position on the grating given by $x_g = B\tan\theta_r$, and from there is reflected at angle θ_i. Light from the grating encounters the mask at normal incidence. Therefore, the relation between θ_r and distance x in the masking plane (Fig. 1) is

$$x = B\tan\theta_r\cos\theta_i,$$

$$dx/d\theta_r = B\sec^2\theta_r\cos\theta_i = R\sec\theta_r\cos\theta_i. \tag{2.3}$$

Combining (2.2) and (2.3), we have

$$\frac{d\lambda}{dx} = \frac{d\cos^3\theta_r}{B\cos\theta_i} = \frac{d\cos^2\theta_r}{R\cos\theta_i}. \tag{2.4}$$

The wavelength dispersion is converted to a dispersion of frequencies in the masking plane through the fundamental relation $c = f\lambda$, which yields

$$df/d\lambda = -c/\lambda^2. \tag{2.5}$$

With our grating of 1200 lines/mm, and within our experimentally useful bandwidth of about 35 Å at 10 647 Å, $d\lambda/dx$ varies by about ± 0.4 percent and df/dx by about ± 0.6 percent. It has not been necessary to account for these small deviations from linearity. Appendix B gives a complete listing of our experimental parameters.

3) Grating Compressor (Quadratic Phase Correction): The grating compresses the chirped pulse by subtracting from the phase a term quadratic in the frequency deviation. This term has the form

$$\Phi_c = a_0(\omega - \omega_0)^2. \tag{2.6}$$

As derived by Treacy [10] and later elucidated by Martinez *et al.* [11], the coefficient a_0 is given by

$$a_0 = \frac{2R_0\lambda_0^3}{4\pi c^2 d^2 \cos^2\theta_0}. \tag{2.7}$$

To understand this formula, let $2R_0 = 2B/\cos\theta_0$ be the double-pass path length for the wavelength λ_0, diffracted with k vector at angle $\theta_r = \theta_0$. As indicated in [11], the essence of the phase correction lies in the fact that the phase fronts of plane waves of neighboring k vector, diffracted at angle $\theta_r \neq \theta_0$, intersect the same point with the *shorter* path length $P = 2R_0\cos(\theta_r - \theta_0)$. Since the phase is $\phi = 2\pi P/\lambda$, differentiation and evaluation of the derivative at $\theta_r = \theta_0$ yields

$$\frac{d^2\phi}{d\omega^2} = \frac{\lambda^3}{2\pi c^2}\cdot\frac{d^2P}{d\lambda^2} = -\frac{2R_0\lambda_0^3}{2\pi c^2}\left(\frac{d\theta_r}{d\lambda}\right)^2. \tag{2.8}$$

The quadratic coefficient is $a_0 = -\frac{1}{2}(d^2\phi/d\omega^2)$. Hence, in view of (2.2), (2.7) follows.

III. Frequency Filter (Effects of Mask and Spot Size)

Having represented the chirped pulse in the time domain, the remaining steps in the analysis are to transform to the frequency domain, apply the appropriate filter functions to account for the grating and mask, and transform back to the time domain to see the shaped and compressed output pulse. The filtering by the grating is assumed to be a pure quadratic phase correction, as indicated by (2.6) and (2.7).

The amplitude and phase transmission of the mask in position space is represented by a complex function $M(x)$. Because of the finite spot size on the mask, the filter function in *frequency* space is a smeared image of the spatial masking function $M(x)$; for the same reason, diffraction from sharp edges on the mask deflects some of the energy flux off axis. This section properly accounts for these effects of the finite spot size.

We define $B(x, y)$ as the electric field profile at the mask for the particular frequency ω_0 whose distribution is centered at $x = 0$, $y = 0$. Then the profile for any frequency ω is $B[x - \alpha(\omega - \omega_0), y]$ where $\alpha \equiv dx/d\omega = -\lambda^2/[2\pi c(d\lambda/dx)]$. We also define

$$\Omega = \omega - \omega_0$$

$$\exp(-ja_0\Omega^2) = \text{quadratic phase correction of grating}$$

$$E(\Omega) = \text{Fourier transform of chirped pulse envelope } \hat{E}_{ch}(t) \text{ [12]}$$

$$= \int dt \exp(-j\Omega t)\,\hat{E}_{ch}(t)$$

where the chirped pulse field with the carrier is the real part of $E_{ch}(t) = e^{j\omega_0 t}\,\hat{E}_{ch}(t)$. Then the envelope of the masked field can be represented as

$$E(\Omega, x, y) = E(\Omega)\, e^{-ja_0\Omega^2}\, M(x)\, B(x - \alpha\Omega, y). \tag{3.1}$$

We adopt the following procedure for relating $M(x)$ to an effective frequency filter function $S(\Omega)$. First, we expand the masked field $E(\Omega, x, y)$ in Hermite–Gaussian modes. The higher modes diffract to larger angles and, to a good approximation, are lost because of spatial filtering in the experimental setup. Therefore, we take the filter function $S(\Omega)$ to be the coefficient of the lowest Hermite–Gaussian mode in the expansion of $M(x)\,B(x - \alpha\Omega, y)$.

The expansion of $E(\Omega, x, y)$ in Hermite–Gaussian modes has the form [13]

$$E(\Omega, x, y) = \sum_{m,n} A_{mn}(\Omega)\, u_{mn}(x - \alpha\Omega, y) \tag{3.2}$$

with coefficients A_{mn} and eigenmodes u_{mn}. In the present case, we take the incoming beam profile itself to be the lowest order mode which, with $X \equiv x - \alpha\Omega$, can be written as

$$B(X, y) = u_{00}(X, y)$$

$$\equiv (2/\pi w_0^2)^{1/2}\exp[-(X^2 + y^2)/w_0^2] \tag{3.3}$$

where w_0 is the $1/e$ field radius of the spot at the mask. This same w_0 is then a natural and appropriate parameter in (3.2). In this case, the formula [13] for the lowest order coefficient in (3.2) reduces to

$$A_{00}(\Omega) = E(\Omega)\exp(-ja_0\Omega^2)\, S(\Omega) \tag{3.4}$$

where $S(\Omega)$, the frequency filter transfer function ascribed to the mask, is

$$S(\Omega) = (2/\pi w_0^2)^{1/2}\int_{-\infty}^{\infty} M(x) e^{-2(x-\alpha\Omega)^2/w_0^2}\, dx. \tag{3.5}$$

The formula shows that the mask weighting in frequency space is the mask weighting in x-space, convolved with the *intensity* profile of the beam, i.e., convolved with a Gaussian beam profile of effective spot size $w_0/(2)^{1/2}$, w_0 being the actual field spot size.

To the present approximation, the space dependence of the output pulse is given by the lowest Hermite–Gaussian mode, and $A_{00}(\Omega)$ is the Fourier transform of the tailored output pulse [14], [15]. The inverse Fourier transform of $A_{00}(\Omega)$ gives the pulse shape in the time domain. Since

the factor multiplying $S(\Omega)$ in (3.4) is just the Fourier transform of the compressed pulse without masking, the result in the time domain is the convolution of that pulse with the impulse response of the filter $S(\Omega)$. From (3.5), the impulse response of $S(\Omega)$ is

$$s(t) = m(t)\, g(t) \tag{3.6}$$

where $m(t)$ is the impulse response of the *infinite-resolution* filter $M(\alpha\Omega)$, given by

$$m(t) = \frac{1}{2\pi} \int_{-\infty}^{\infty} d\Omega e^{j\Omega t} M(\alpha\Omega) \tag{3.7}$$

and $g(t)$ is the Gaussian weighting or *envelope* function

$$g(t) = \exp\,(-w_0^2 t^2/8\alpha^2). \tag{3.8}$$

Finally, the electric field envelope of the tailored output pulse is

$$a_{00}(t) = e(t)^*[m(t) \exp\,(-w_0^2 t^2/8\alpha^2)] \tag{3.9}$$

where $e(t)$ is the electric field envelope of the compressed pulse with no masking and where * denotes convolution. Equation (3.9) explicitly shows the effect of the finite spot size in restricting the time window in which the tailored output pulse can accurately reflect the response of the infinite-resolution mask. The effect (subject to the previously stated assumptions) is to multiply $m(t)$ by a Gaussian envelope whose intensity full width at half maximum (FWHM) is $4\alpha(\ln 2)^{1/2}/w_0$. With our setup parameters as given in Appendix B ($\alpha \approx 1.05$ mm·ps, $w_0 \approx 0.3$ mm), the above FWHM is 11.6 ps. Improvement of the resolution is discussed in Section VII.

IV. Examples of Simple Masks

A. Semi-Infinite Screen

Consider a mask that completely blocks light falling on $x < x'$ and passes without change light falling on $x > x'$, i.e.,

$$\begin{aligned} M(x) &= 0 \quad \text{for} \quad x < x', \\ M(x) &= 1 \quad \text{for} \quad x > x'. \end{aligned} \tag{4.1}$$

Then (3.5) yields, with $\Omega' \equiv x'/\alpha$,

$$S(\Omega) = \frac{1}{2}\left[1 - \operatorname{erf} \frac{(2)^{1/2}\,\alpha(\Omega' - \Omega)}{w_0}\right]. \tag{4.2}$$

In the infinite resolution limit, this mask would block frequencies $\Omega < \Omega'$ and pass $\Omega > \Omega'$. Equation (4.2) tells us that the effects of the finite spot size w_0 are to "soften" the cutoff at Ω' and reduce the *field* at $\Omega = \Omega'$ to one half of the unmasked value. Therefore, a mask designed to block $\Omega < \Omega'$ and pass $\Omega > \Omega'$ reduces the observed *intensity* associated with Ω' to one quarter of its original value.

This paradoxical result deserves thought. Certainly, half the power associated with Ω' gets past the semi-infinite screen. The difference between one quarter and one half is accounted for by diffraction: the higher order Hermite–Gaussian modes are diffracted to larger angles by the sharp boundary at $x = x'$ and presumably eliminated by spatial filtering in the setup.

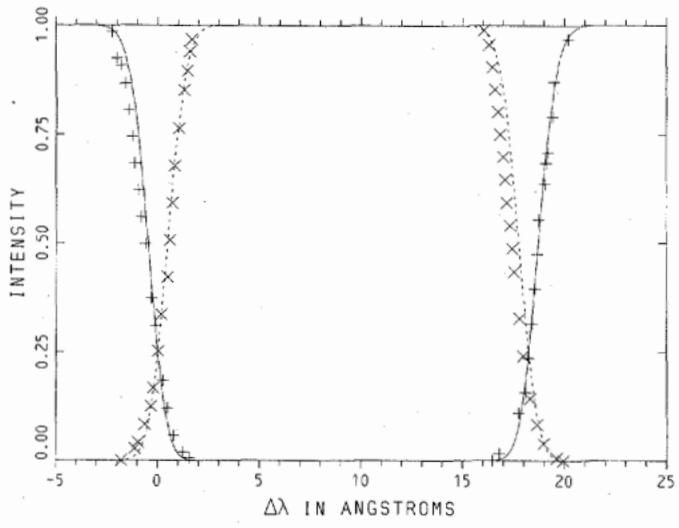

Fig. 2. Superposition of calculated power spectra $|S(\Omega)|^2$ masked by a 1/8 in wire (solid curve) and a 1/8 in slit (dashed curve), and corresponding experimental points (+ for wire and × for slit). The wire blocks more of the spectrum than is passed by the slit. Spot size $w_0 = 0.30$ mm.

The frequency that has half of its original power remaining in the lowest mode belongs to a position out in the beam about a quarter spot size away from the edge [16]. In this sense, the edge is the quarter-power position for the lowest mode, while the half power position is shifted about a quarter spot size outward into the beam.

A consequence of this result is that when looking at the half power points in masked spectra, opaque strips blocking portions of the spectrum appear wider and slits appear narrower than their true widths, the "true" widths being obtained by multiplying $d\lambda/dx$ times the actual width in x. An opaque strip blocks more of the spectrum than is passed by a slit of the same width. An experimental confirmation of this effect is presented in Section V-A and Fig. 2.

B. Array of Strips

Let a mask consist of a pattern of s strips. Let t_j denote the constant complex value of $M(x)$ for the jth strip which has edges at x_j and x_{j+1}. Then the contribution of strip j to the integral in (3.5) is

$$S_j(\Omega) = \tfrac{1}{2}\, t_j[\operatorname{erf}\,(\eta_{j+1} - \eta) - \operatorname{erf}\,(\eta_j - \eta)] \tag{4.3}$$

where

$$\eta_j \equiv (2)^{1/2}\, x_j/w_0, \quad \eta = (2)^{1/2}\, \alpha\Omega/w_0. \tag{4.4}$$

The contribution of all the strips is

$$S(\Omega) = \sum_{j=1}^{s} S_j. \tag{4.5}$$

If the strips are wide compared to the spot size, then $S(\Omega)$ is essentially equal to t_j over most of the frequency range intercepted by strip j, and there are soft edges at the transitions to the values of the neighboring strips. At the other extreme, if the strips are narrow compared to the spot size, neighboring strips have an influence over an entire strip width, and the stepwise variations of $M(x)$ are smoothed out so that no edges are apparent in $S(\Omega)$.

C. Simple Window

A centered simple window with edges at $x_s = \alpha\Omega_s$ and $-x_s$ can be viewed as a single strip with unity transmission over the strip and zero outside. Its $S(\Omega)$ is given by (4.3), which merely expresses how the edges of the transfer function are softened. It is more instructive to look at the response in the time domain from the point of view of (3.9). The impulse response envelope of the *infinite-resolution* filter $M(\alpha\Omega)$ is, from (3.7),

$$m(t) = \frac{\Omega_s \sin(\Omega_s t)}{\pi\Omega_s t}. \tag{4.6}$$

The impulse response envelope of the effective filter $S(\Omega)$ is $m(t)$ multiplied by the Gaussian envelope of (3.8). Finally, the electric field envelope of the windowed output pulse is

$$a_{00}(t) = e(t)^* \left[\frac{\Omega_s \sin(\Omega_s t)}{\pi\Omega_s t} \exp\left(-w_0^2 t^2/8\alpha^2\right)\right]. \tag{4.7}$$

Equation (4.7) shows that the windowed output pulse is the convolution of the unwindowed pulse with the product of the Gaussian weighting envelope and the indicated $m(t)$.

V. Comparisons with Experiment

A. Spectra with Slit and Wire of Same Width

To test our treatment of the finite spot size and to confirm the parameters used in the model, power spectra were recorded with a $\frac{1}{8}$ in slit in the masking plane, and also with a $\frac{1}{8}$ in diameter opaque wire. Fig. 2 shows points along the edges created by the slit and wire indicated as experimental points to be compared with calculated curves of the intensity weighting (which is the square of the filter function). Both the experimental and calculated values for the slit and wire cross at the quarter-power points, as predicted. As predicted, the slit does indeed appear narrower (at half power) than the wire.

These comparisons show that the parameters $d\lambda/dx$ and spot size, determined as explained in Appendix B, are correct. If the relation between λ and x were wrong, only one edge would line up with the experimental points. If the spot size were wrong (or if our method of handling it were wrong), the slope would not be right.

B. Simple Windowing

The first application of masking in a grating compressor was simple spectral windowing to eliminate the pulse wings [3]. Calculations qualitatively confirm the improvement resulting from windowing. Fig. 3 shows the calculated spectra and calculated output pulse autocorrelations, illustrating the improvement obtained by windowing a 44 Å spectrum down to 34 Å by a 6.1 mm window. The improvement, which is in good agreement with that obtained experimentally [3], [4], is due to eliminating a portion of the spectrum that is not linearly chirped.

C. Periodically Spaced Wires

A spatially periodic interruption of the spectrum yields a sequence of pulses whose spacing in time is inversely proportional to the spatial period. Figs. 4 and 5 show the experimental [1] and calculated results for a mask of periodically spaced wires, windowed to pass six peaks of the spectrum, and then windowed still more to pass undiminished only two of the peaks. As illustrated by Fig. 5, the time width of the individual pulses is inversely proportional to the bandwidth.

The spot size affects the fine features of the spectrum, and as shown by (3.9), controls the width of an envelope over the pulse heights in the time domain. We have found that if a spot size 60 percent too large is used in the calculations, the effect on the spectrum is just barely noticeable, but the peaks adjacent to the central peak in the pulse autocorrelation are drastically reduced in height. In the upper, 3.2 mm window case of Fig. 5, the side peaks were reduced from about $\frac{2}{3}$ to less than $\frac{1}{3}$ of the height of the central peak. This result is far more sensitive than the experiment of Fig. 2 in testing whether the calculation is using the correct spot size.

D. Odd Pulse

If half of an originally symmetric spectrum undergoes a π phase shift, it becomes an antisymmetric spectrum. The electric field in the time domain is an odd function of time. The intensity profile has two peaks with a null at $t = 0$ where the phase jumps by π. For example, the inverse transform of an $E(\Omega)$ that is -1 from $-\Omega_s$ to 0 and $+1$ from 0 to Ω_s is proportional to $(\sin^2\Omega_s t)/(\Omega_s t)$. The resulting *intensity* envelope, proportional to $(\sin^4\Omega_s t)/(\Omega_s t)^2$, has peaks at $\Omega_s t = \pm 1.1656$.

An odd pulse can be achieved experimentally by introducing a plate that shifts the phase by an odd multiple of π over half the spectrum [17]. Fig. 6 shows a calculated odd pulse power spectrum and pulse intensity, and calculated and experimental [1] autocorrelations. Even though all the power goes through the mask, the power spectrum has a hole at the center frequency because none of the power associated with that frequency appears in the lowest order (''on-axis'') Hermite–Gaussian mode.

E. Square Pulse

The production of a square pulse envelope requires a frequency filter $S(\Omega)$ proportional to $(\sin\Omega\tau)/(\Omega\tau)$ [18]. A truncated $(\sin kx)/kx$ mask was approximated as described by Weiner *et al.* [4]. The amplitude variations were accomplished by alternating opaque and transmitting strips whose widths, always small compared with the spot size

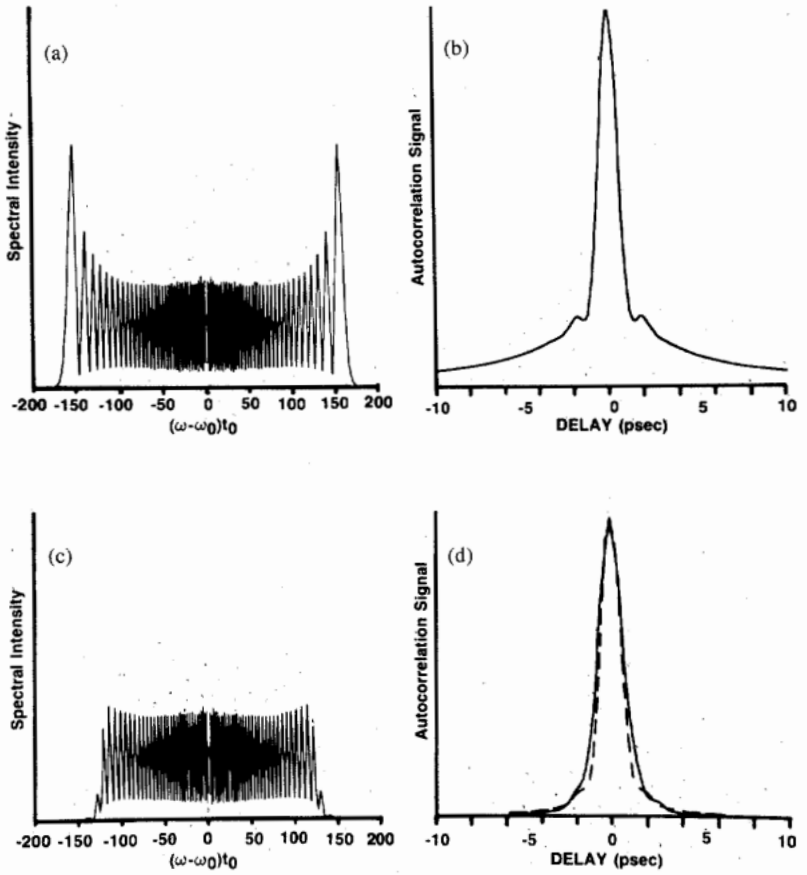

Fig. 3. Improvement in output pulse autocorrelation obtained by spectral windowing. (a) Raw power spectrum (calculated). (b) Calculated autocorrelation of output pulse from (a). (c) Power spectrum with 6.1 mm window (calculated). (d) Calculated autocorrelation of output pulse from (b) (dashed) and experimental comparison (solid). Chirped pulse calculated from (A7) and (A8) with $A = 280$, $z/z_0 = 0.0024$ ($z = 450$ m, $z_0 = 190$ km at 1.064 μm from [2, Fig. 10] $\gamma = 37$ for 1.71 dB/km. From FFT, FWHM $t_0\Delta\Omega = 320.7$, which with $\tau_0 = 78$ ps and $t_0 = \tau_0/1.76$ corresponds to FWHM $\Delta\lambda = 43.6$ Å. Compressed pulses calculated with quadratic phase factor $a_0/t_0^2 = 0.0035$. Calculated compressed pulse FWHM 0.97 ps both with and without 6.1 mm window. Window width of 6.1 mm intercepts 35 Å based on $d\lambda/dx = 5.743$ Å/mm. FFT gave FWHM of windowed power spectrum $t_0\Delta\Omega = 247.1$ or $\Delta\lambda = 33.6$ Å.

in order to give a smooth $S(\Omega)$, were adjusted to produce the desired variation. The needed π phase shifts were obtained by etching strips of appropriate depth on a separate mask placed in series with the first.

Fig. 7 shows the calculated power spectrum as filtered by this mask, the calculated output pulse intensity, and for comparison, calculated and experimental output pulse cross correlations with a compressed pulse obtained from a spectrum that is simply windowed.

The inverse transform of

$$F(\Omega) = 2\tau \sin(\Omega\tau)/\Omega\tau$$

is an envelope function $f(t)$ that is 1 on $-\tau < t < \tau$ and 0 for $|t| > \tau$. In the pulse tailoring setup, $F(\Omega)$ is necessarily truncated because of the finite bandwidth available in the chirped pulse. It is interesting to see the effect on the pulse shape of varying the number of periods of sin $(\Omega\tau)$ that are included in a window of fixed frequency width. With window (or slit) edges at $-\Omega_s$ and $+\Omega_s$, there is a zero of sin $(\Omega\tau)$ at each edge when $\tau = n\pi/\Omega_s$, $n = 1, 2, 3, \cdots,$. In the untruncated case (Ω_s a parameter, but infinite spectral width), the "square" output pulse should simply get longer (proportional to n) as n is increased. In the windowed case, it should also become more nearly square, as we are including more features of the ideal sin $(\Omega\tau)/\Omega\tau$ spectrum. Because the central spectral intensity remains fixed when masking with $\sin(kx)/kx$ masks, the output pulse intensity is expected to drop off roughly as $1/\tau^2$, i.e., $1/n^2$.

Fig. 8 shows the calculated output pulse shapes that result from $\sin(kx)/kx$ masks with k adjusted to provide various values of n in the formula $\tau = n\pi/\Omega_s$, Ω_s fixed. The pulse shape is seen to improve only up to $n = 4$. The deterioration for $n > 4$ is due to insufficient resolution at the mask. The 33 Å spectrum used in this calculation is about 5.7 mm wide. For $n = 5$, a change of π in $\Omega\tau$ corresponds to only 1.9 spot sizes, and the effective mask (frequency filter) is strongly distorted from the ideal sin

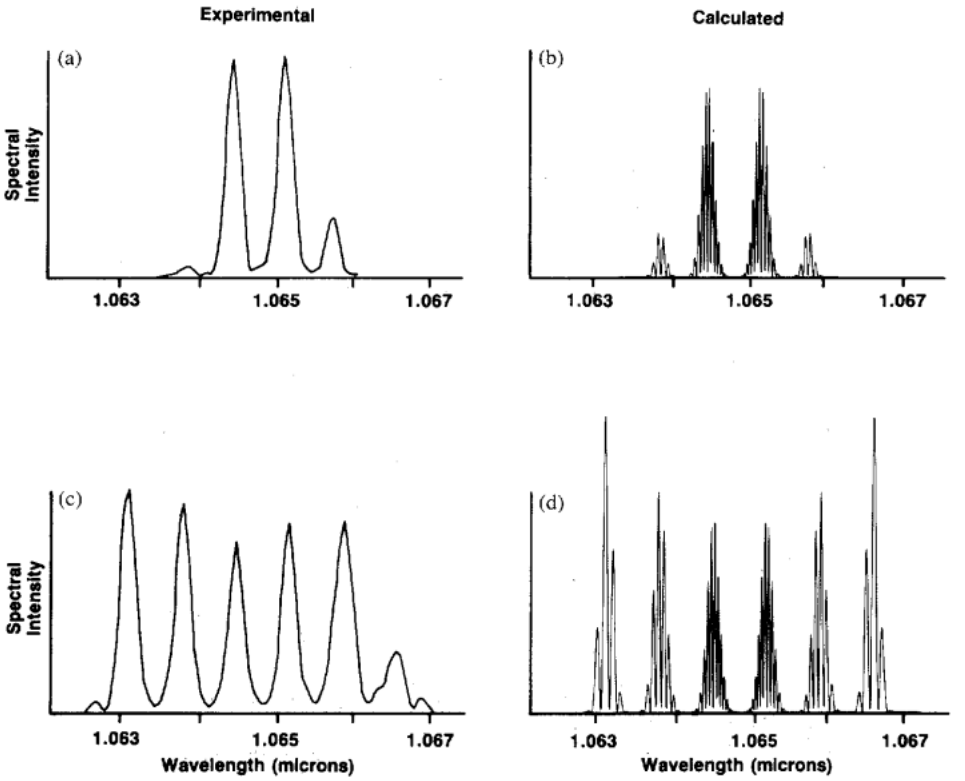

Fig. 4. Experimental and calculated power spectra with a spatially periodic mask that consists of 0.8 mm diameter wires spaced about 1.1 mm center to center with windows of various widths. (a) and (b) 3.2 mm window (three wires exposed). (c) and (d) 7.4 mm window (seven wires exposed). The fine structure is not resolved in the experimental spectrum which is averaged over many pulses that are all subject to various small fluctuations.

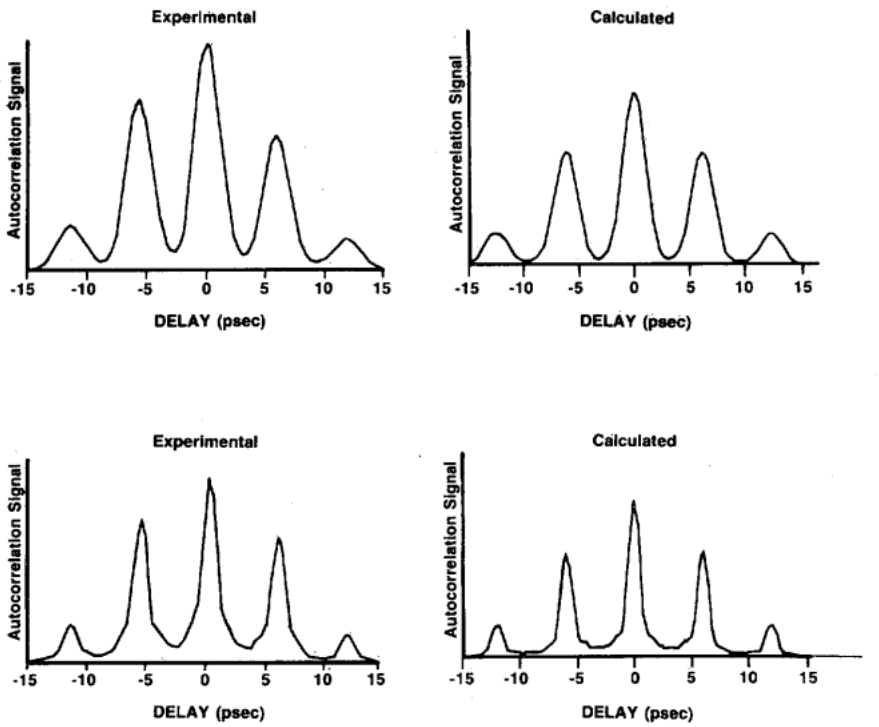

Fig. 5. Experimental and calculated pulse autocorrelations for the masks that yielded the power spectra in Fig. 4. Upper: 3.2 mm window. Lower: 7.4 mm window.

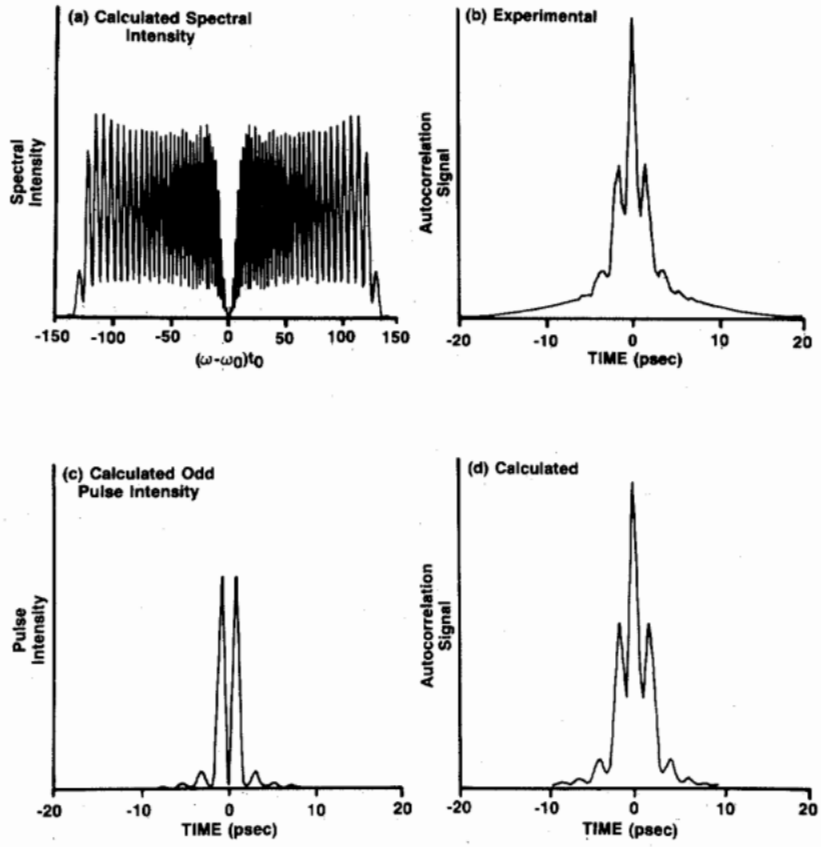

Fig. 6. Odd pulse (a) calculated spectral intensity, (b) experimental autocorrelation, (c) calculated odd pulse, (d) calculated autocorrelation. The tails are prominent in (b) because no window was used. Calculation used window of Fig. 3(c).

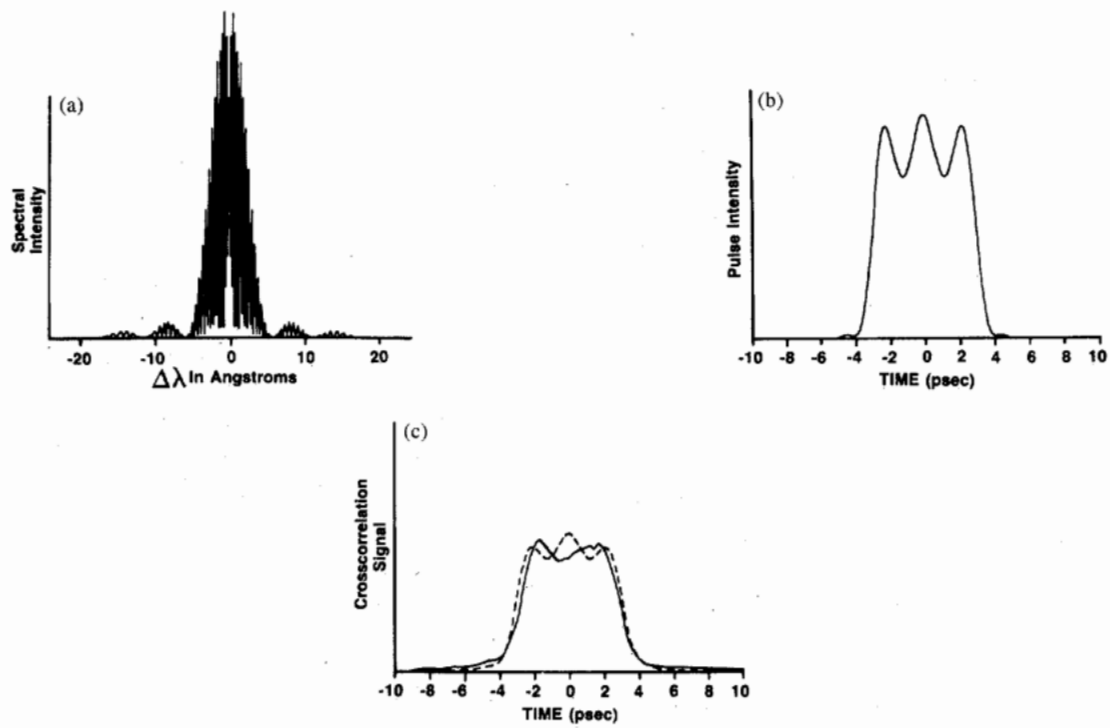

Fig. 7. Square pulse (a) calculated spectral intensity from mask described in [4]. (b) Calculated pulse from above mask. (c) Calculated cross correlation with simply windowed pulse (dashed) and experimental cross correlation (solid).

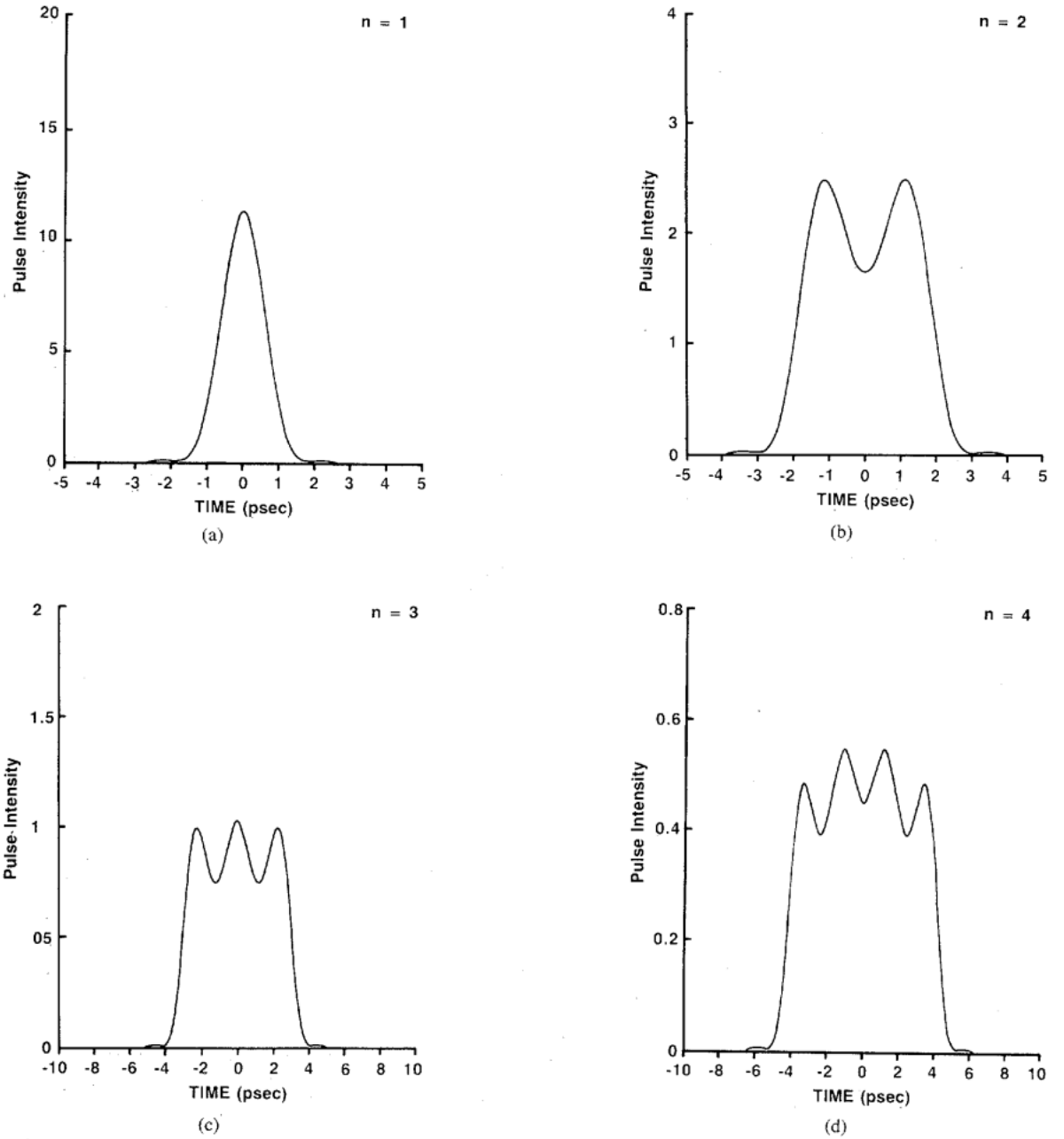

Fig. 8. Calculated "square" pulses from sin $(kx)/kx$ masks with k adjusted such that the range of kx over the window of fixed width is $2n\pi$, $n = 1, 2, 3, 4, 5, 6$. Spot size $w_0 = 0.3$ mm. Window width = 5.74 mm (33 Å or 0.87 THz). The corresponding square pulse widths for infinite bandwidth are given by $2\tau = (2n/0.87)$ ps or 2.3, 4.6, 6.9, 9.2, 11.5, and 13.8 ps, respectively. The numbers on the vertical axes may be used to compare the intensities.

$(\Omega\tau)/(\Omega\tau)$ shape by the convolution of the $\sin(kx)/(kx)$ mask with the intensity profile of the beam in (3.5.). From the viewpoint of (3.9), the increase in $\tau = n\pi/\Omega_s$ has broadened the tailored pulse so much that the Gaussian time envelope strongly affects the shape.

Parenthetically, we note that for a flat incident pulse spectrum and infinite spectral resolution, the resulting field envelope shapes are the result of putting an ideal square pulse of duration 2τ through a low-pass filter with a sharp cutoff at Ω_s, and may be expressed analytically (with $\tau = n\pi/\Omega_s$) as

$$f(t) = \frac{1}{\pi\tau}\{\mathrm{Si}[\Omega_s(t+\tau) - \mathrm{Si}[\Omega_s(t-\tau)]\}.$$

Here Si denotes the sine integral function, defined by $\mathrm{Si}(x) = \int_0^x [\sin(u)/u]\, du$. The outer peaks in Fig. 8 (for $n > 1$) reflect the familiar overshoot phenomenon, depressed by the Gaussian time envelope.

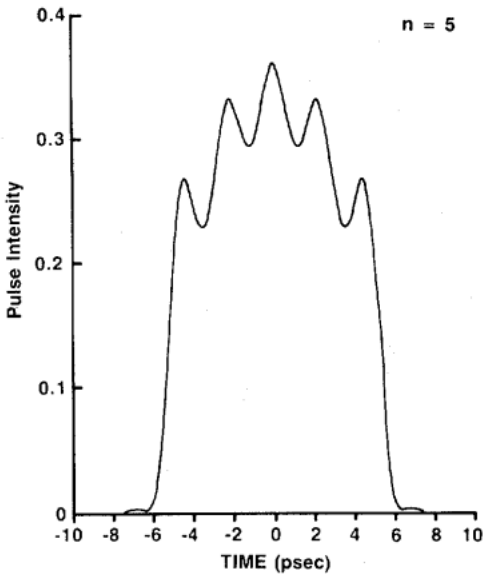

(e)

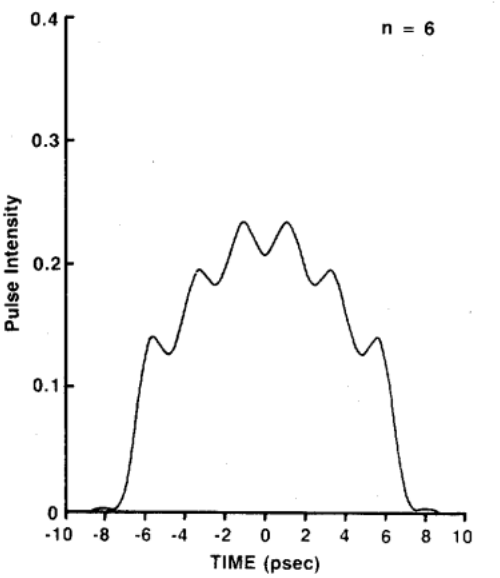

(f)

Fig. 8. (*Continued.*)

VI. Additional Pulse Shapes

The pulse shapes that can be synthesized are subject only to the limitations of spectral bandwidth of the chirped pulse and spatial resolution at the mask. The shapes that will find application remain to be determined. Nevertheless, it seems appropriate to give one example that is easy to calculate, but has not been synthesized experimentally.

A. Two Square Pulses with a Space Between Them

The transform of two rectangular pulses of duration 2τ with a space of duration 2τ between them is proportional to $[\sin(\Omega\tau)/\Omega\tau]\cos(2\Omega\tau)$ [18]. Fig. 9 shows, for four different spot sizes, the calculated results when our chirped pulse encounters a $[\sin(kx)/kx]\cos(2kx)$ mask with no transmission for $|kx| > 3\pi$. This example again illustrates the degradation due to spot-size-limited resolution that was already seen for $n > 4$ in Fig. 8. Because of the longer duration ($6\tau \approx 20$ ps) associated with the rapid variations of $\cos(2kx)$, resolution is more critical than with a single square pulse of duration 2τ. The Gaussian envelope of (3.9) depresses the leading and trailing corners, but leaves the sharp hole in the center. As the spot size is reduced, the envelope broadens until, for $w_0 = 0.06$ mm in this example [Fig. 9(d)], its effect is barely noticeable.

VII. Spectral Resolution

It is useful to define a measure of the spectral resolution of our setup as

$$m \equiv \Delta x/w_0 \tag{7.1}$$

where $\Delta x = \alpha\Delta\omega = \Delta\lambda/(d\lambda/dx)$ is the length on the mask of the useful spectral width $\Delta\lambda$ (of radian frequency width $\Delta\omega$) and the "spot size" w_0 is, as in (3.3), the $1/e$ field radius of the beam. This resolution measure m is proportional to the number of consecutive bandwidth-limited features that can be synthesized in a single tailored pulse in the time domain. For example, a Gaussian spectral distribution of intensity FWHM $\Delta\omega$ would allow fine structure in the time domain of the transform-limited intensity FWHM $\Delta t = 4\cdot\ln(2)/\Delta\omega$. The Gaussian envelope in (3.9) limits the tailored pulse duration to an intensity FWHM of $\Delta T = 4\alpha(\ln 2)^{1/2}/w_0$. Thus, the number of fine features that can be contained in a single tailored pulse is proportional to [19]

$$\frac{\Delta T}{\Delta t} = \frac{\Delta x}{w_0(\ln 2)^{1/2}} \approx 1.2m. \tag{7.2}$$

Let us see how large m can be. In the setup of Fig. 1, we see that w_0 at the mask is related to the beam radius w at the lens L of focal length f by the Gaussian beam optics relation

$$\pi w w_0 = \lambda f. \tag{7.3}$$

Writing $\Delta x = \Delta\lambda/(d\lambda/dx)$ and taking $d\lambda/dx$ from (2.4), we obtain

$$m = \frac{\Delta\lambda}{\lambda}\cdot\frac{\pi w}{d}\cdot\frac{R}{f}\cdot\frac{\cos\theta_i}{\cos^2\theta_r}. \tag{7.4}$$

For convenience, in our current setup, the focal length f is substantially greater than the first bounce to second bounce path R. The best resolution would be obtained by moving both the lens L and the mask as close to the grating as possible so that $f \to R$. Equation (7.4) reveals other ways in which the resolution may be improved for a fixed $\Delta\lambda/\lambda$: larger input spot w, smaller line spacing d on the

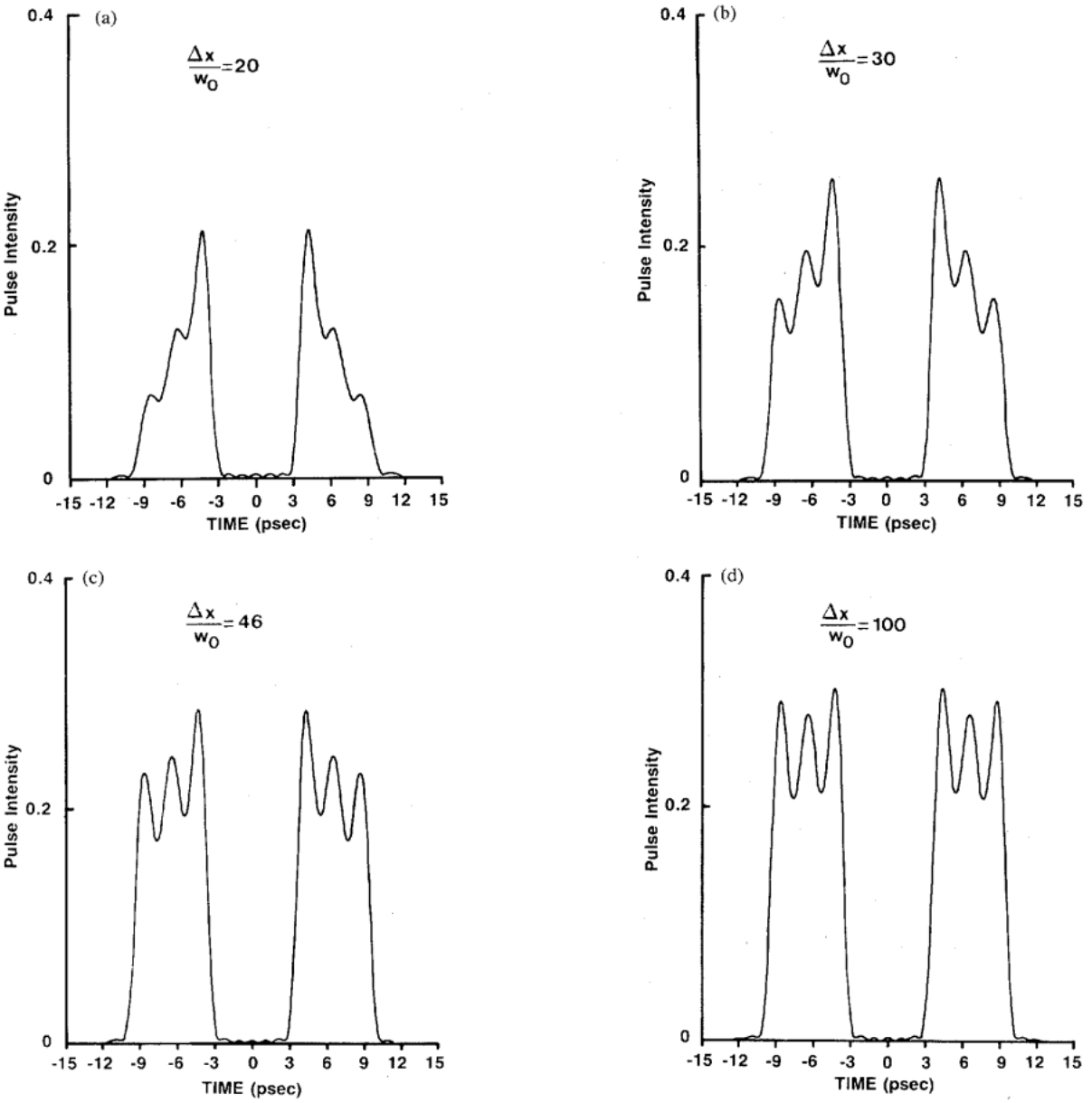

Fig. 9. Pulses resulting from sin (kx) cos ($2kx$)/kx mask $|kx| \leq 3\pi$ for four different spot sizes. The theoretical result from the untruncated sin ($\Omega\tau$) cos ($2\Omega\tau$)/$\Omega\tau$ frequency filter is two square pulses of duration 2τ with a space of duration 2τ between them. Here τ = 3.34 ps. (a) w_0 = 0.3 mm. (b) w_0 = 0.2 mm. (c) w_0 = 0.13 mm. (d) w_0 = 0.06 mm. The four examples correspond to the resolution measure (7.1) m = 20, 30, 46, and 100, respectively.

grating, and optimization of the geometric factor ($\cos \theta_i / \cos^2 \theta_r$). Of course, λ, d, θ_i, and θ_r interact through (2.1) (or its generalization if a different spectral order is used). We note here that maximization of $\cos \theta_i / \cos^2 \theta_r$ has the tradeoff that working too near to $\theta_r = 90°$ may cause $d\theta r / d\lambda$ to vary significantly over the band and lead to unwanted temporal dispersion.

Our current experimental resolution is obtained from the measured values of $\Delta\lambda$, $d\lambda/dx$, and w_0. With $d\lambda/dx$ = 5.743 Å/mm (see Appendix B for values of the essential parameters), our windowed spectrum of 35 Å has a width at the mask of about 6 mm or m = 20 spot sizes with w_0 = 0.3 mm. Table I shows the resolution parameters of the present setup, which has not been optimized, and of some variations with improved resolution. The table is constructed for the indicated constant values of $\Delta\lambda$, λ, input spot size w, and quadratic coefficient a_0. The first row summarizes the parameters of the present setup with m = 20. The second row indicates the maximum improvement resulting from reducing f to R without changing d or the angles. The third row illustrates the effect of the geometric factor, improving m from 46 to 64 by interchanging θ_i and θ_r from row 2. Throughout the table, R is scaled to keep the same a_0 in (2.7). Row 4 predicts the drastic improvement to m = 120 obtained by using a grating with 1800 lines/mm instead of the present 1200.

TABLE I
RESOLUTION PARAMETERS. $\Delta\lambda = 35$ Å, $\lambda = 1.06$ μm, $w = 3.4$ mm, $a_0 = 6.16$ ps^2.

Description[a]	$\frac{1}{d}$ (mm)$^{-1}$	θ_i	θ_r	$\cos\theta_i/\cos^2\theta_r$	f (m)	R (m)	Δx (mm)	w_0 (mm)	m
Present Setup	1200	43.55°	36°	1.11	3.01	1.31	6.1	0.3	20
$f = R$	1200	43.55°	36°	1.11	1.31	1.31	6.1	0.13	46
$f = R$	1200	36°	43.55	1.54	1.05	1.05	6.8	0.11	64
$d = 555$ nm, $f = R$	1800	77.29°	70°	1.88	0.104	0.104	1.23	0.01	120

[a] Row 3 interchanges the θ_i and θ_r of row 2.

An 1800 line/mm grating has been used to compress 1.06 μm pulses, and the tremendous reduction of R (to 10.4 cm in Table I) that results from operation near grazing incidence has been noted [20]. The width of the 35 Å spectrum on the mask is now reduced to only 1.23 mm, but the spot size w_0 is reduced still further, to only 10 μm. Note, however, that the smaller mask requires closer tolerances. Interchange of θ_i and θ_r to further exploit the geometric factor would lead to still better diffraction-limited resolution, but at the expense of a substantial increase in unwanted higher order dispersive effects from the grating. While it may not be practical to achieve the diffraction-limited resolution implied when $f = R$, that is the *fundamental* limit, and it is clear from the examples in Table I that the resolution can be improved substantially over the present $m = 20$. An m of 100 with the present $\Delta t \cdot \Delta f$ of about 0.8 would, in principle, permit the synthesis of, for example, a 60 ps pulse with 60 1-ps features on it.

VIII. CONCLUSIONS

We have developed and tested a computational tool that accurately predicts the pulse shapes produced when amplitude and phase masks are used to filter the spatially dispersed Fourier components of an optical pulse in a fiber-and-grating pulse compressor. A significant new analytical contribution relates the physical mask to the frequency filter that it produces, accounting for diffraction from the physical mask and finite beam diameter. Spectra and temporal pulse shapes corresponding to a variety of physical masks have been calculated and are found to be in excellent agreement with experiment. We have discussed the limitation that finite spatial resolution imposes on the pulse shapes that can be produced, and we have shown that the attainable resolution can be far better than was achieved in the present experiments. Our analytical results are applicable to other wavelength and time scales, and are easily extended to systems with transmission gratings or prisms. By designing an experiment to optimize resolution, it will be possible to synthesize, to specifications, complex optical pulse shapes with a multitude of picosecond and subpicosecond fine features in the pulse profile.

APPENDIX A
SIMULATION OF CHIRPED PULSE

At the fiber input, before the pulse is chirped, its electric field can be represented as the real part of [2]

$$E_i(t) = E_0 \operatorname{sech}(t/t_0)\, e^{j\omega_0 t}. \tag{A1}$$

The value of t/t_0 for which $\operatorname{sech}^2(t/t_0) = 0.5$ is $t/t_0 = 0.88137$, and hence t_0 is related to the intensity full width at half maximum (FWHM) τ_0 by $\tau_0 = 1.7627\, t_0$. Let the chirped pulse at the fiber output be represented as the real part of

$$E_{ch}(t) = T_{ch}(t)\, e^{j[\omega_0 t - \phi(t)]}. \tag{A2}$$

A. SPM Only

In the SPM-only approximation, we assume that $T_{ch}(t) = E_0 \operatorname{sech}(t/t_0)$ and

$$\phi(t) = G \operatorname{sech}^2(t/t_0) \tag{A3}$$

since $\phi(t)$ is assumed to be proportional to the optical power. G, a coefficient that contains the entire time-independent part of (A3), is expressed in terms of physical quantities in (A6) below. The dimensionless instantaneous frequency $t_0 d\phi/dt$ has extremal values of $4\sqrt{3}\, G/9$, and hence the full spread of the instantaneous radian frequency ω is given by

$$t_0 \Delta\omega = 8\sqrt{3}\, G/9. \tag{A4}$$

The value in (A4) comes very close to the FWHM of the Fourier transform of $E_{ch}(t)$. In the SPM-only approximation, there are only two free parameters. We choose t_0 to agree with the intensity FWHM of the input pulse to the fiber, $\tau_0 = 1.76 t_0$, and then choose G to obtain a spectrum of the same width as the experimental one.

By comparison of (A3) with equations given by Stolen and Lin [6], we find

$$G = \frac{2\pi z}{\lambda} \cdot \frac{1}{2} n_2 E_0^2. \tag{A5}$$

Here z is the fiber length, λ is the vacuum wavelength, and n_2 is the nonlinear coefficient.

The peak electric field amplitude E_0 can be deduced from power measurements and the effective cross-sectional area for the mode propagating in the fiber. If I_0 denotes the peak power per unit area (averaged over the optical period), then in cgs units, $E_0^2 = 8\pi I_0/nc$, $I_0 = 10^7 P/A_{\text{eff}}$ where P is the peak power in watts (so that $10^7 P$ is in ergs/second) and we have

$$G = \frac{2\pi z}{\lambda} \cdot \frac{1}{2} n_2 \frac{8\pi P \cdot 10^7}{ncA_{\text{eff}}}. \tag{A6}$$

Reference [7] (Appendix, note f) is helpful in relating A_{eff} to the fiber core diameter, core-cladding index difference, and wavelength. Equation (A6) enables one to check whether the value of G needed to produce the experimentally observed spectral width is consistent with the measured average optical power, fiber parameters, input pulse width, and pulse repetition rate.

B. Propagation Calculation

The other approach to representing the chirped pulse is to solve numerically the dimensionless nonlinear complex Schrödinger equation that governs the propagation, including group velocity dispersion, namely [9], [2],

$$\frac{\partial u}{\partial(z/z_0)} = -i\frac{\pi}{4}\left[\frac{\partial^2 u}{\partial(t/t_0)^2} - 2|u|^2 u\right] - \gamma u. \quad \text{(A7)}$$

Here u is a complex dimensionless optical field amplitude, γ is a loss coefficient, t is a retarded time, defined such that for any distance z along the fiber, the center of the pulse is at $t = 0$, and the pulse envelope height at $z = 0$ is [2]

$$u(z = 0, t) = A\ \text{sech}(t/t_0). \quad \text{(A8)}$$

The normalization length z_0 and the dimensionless peak amplitude A are defined by [2, eq. (3)–(5)], but in practice we find z_0 from [2, Fig. 10]. Combining [2, eq. (4) and (5)], we obtain

$$A^2 z/z_0 = 2G/\pi \quad \text{(A9)}$$

where G is given by (A6). Having found z_0 and G, one can find A from (A9). A, z/z_0, and the loss coefficient γ are needed as inputs for the propagation calculation from (A7).

Appendix B
Experimental Parameters and Cross Checks

The experimentally measured quantities that are available as inputs to the calculation or as cross checks fall into the categories of 1) fiber properties, 2) laser pulse parameters, 3) setup parameters, 4) power spectra, and 5) compressed pulse autocorrelations and cross correlations.

Our best estimates of quantities in the first three categories and comments on the others are given below.

A. Fiber Properties

$n = 1.46$.
Core cladding $\delta n = 0.0037 \pm 0.0002$.
Loss = 1.71 dB/km ($\gamma = 37$ with $z_0 = 187.5$ km).
D = core diameter = 7.3 μm.
$A_{\text{eff}} = 1.26\,\pi D^2/4 = 52.7\ (\mu\text{m})^2$.
z = length = 450 m.
$n_2 = 1.1 \times 10^{-13}$ esu.

B. Laser Pulse Properties

FWHM $\tau_0 = 78$ ps.
$\lambda = 1064.7$ nm.
$f_r = 10^8$ Hz = pulse repetition frequency.
$P_{\text{AV}} \approx 0.75$ W.
Peak power $P = P_{\text{AV}}/1.13\tau_0 f_r \approx 85$ W.

C. Setup Parameters

Grating period $d = (1/1.2)\ \mu$m (1200 lines/mm).
Angle of incidence $\theta_i \approx 43.55°$.
Angle of refraction $\theta_r \approx 36°$.
Grating separation distance $R = 1.31$ m.
$d\lambda/dx = 5.743$ Å/mm.
$\alpha = d\omega/dx = 1.048$ mm·ps.
Field spot size $w_0 \approx 0.3$ mm at the mask.
Distance from focusing lens to mask ≈ 3.01 m.

After the setup was fixed, it was left unchanged, but the power was adjusted to obtain a clean compressed pulse.

While $d\lambda/dx$ can, in principle, be obtained from (2.4), the more reliable value cited above was determined directly, as follows. Spectra were recorded with a slit placed in the masking plane: a micrometer stage was used to control the position of the slit. The central wavelength passed by the slit was determined for each slit position. The indicated $d\lambda/dx$ was obtained by fitting the wavelength versus position data to a straight line. The consistency of this data suggests that our $d\lambda/dx$ is correct within about 1 percent.

To measure the spot size, the power was turned down to eliminate spectral broadening. The measurement then proceeded in the usual manner by passing a knife edge on a micrometer in front of a power meter receiving the beam. The radius w at the $1/e$ points of the field was then deduced from the power versus knife edge position data.

The value of $\theta_i - \theta_r$ could be estimated to be within about a degree of 6.5°. Use of this result simultaneously with (2.1) and the above values of λ and d give $\theta_i = 43°$ and $\theta_r = 36.5°$, each within about $\pm 0.5°$. Calculation of $d\lambda/dx$ from (2.4) with the above-listed R then gives 5.62 $\pm$ 0.12 Å/mm, a value acceptably close to the directly measured 5.74 Å/mm, which would correspond to $\theta_r = 36°$ and $\theta_i = 43.55°$.

D. Power Sectra

The observed power spectra have a characteristic shape similar to shapes observed by Stolen and Lin [6] and to the calculated shape shown in Fig. 3(a), but are seldom perfectly symmetrical. The asymmetric spectra droop toward the long wavelength side and are asymmetrically broadened toward that side. Because the asymmetry is most evident when the power is increased above the threshold for stimulated Raman scattering (SRS), we attribute the asymmetry primarily to the effect of SRS on the propagating pulse. Only two or three of the peaks near each edge could be resolved. A typical wavelength difference between the outermost peaks was 43 Å, and the FWHM about 45 Å.

With SPM only, the spectrum was simulated (see Appendix A) with $G = 69\pi$, which (with $\tau_0 = 78$ ps) gave a chirped pulse whose FFT had an outermost peak separation of 43.6 Å and an intensity FWHM of 45.1 Å, in acceptably close agreement with the experimental param-

TABLE II
VALUES OF a_0 IN THE CALCULATIONS

Chirp	Value for Max I				Value Used			
	I_{peak}	FWHM (t_0)	a_0/t_0^2	a_0 (ps)^2	I_{peak}	FWHM t_0	a_0/t_0^2	a_0 (ps)^2
SPM only	35.7	0.0176	0.0013	2.54	31.1	0.0200	0.00124	2.43
With GVD	44.6	0.0190	0.00357	6.99	37.5	0.0220	0.0035	6.85

eters. Incidentally, the $\Delta\lambda$ from the instantaneous frequency calculation of (A4) is 45.3 Å, remarkably close to the FFT result.

In the calculation from the nonlinear Schrödinger equation, the inputs $A = 280$, $z/z_0 = 0.0024$, $\gamma = 37$ gave a chirped pulse whose FFT (with $\tau_0 = 78$ ps) had a spectral intensity FWHM of 43.6 Å and an outermost peak separation of 41.9 Å.

For correlation with the measured power and fiber parameters, we calculate $G = 135$ from (A6) and use [4, Fig. 10] to obtain $z_0 = 190$ km at 1.06 μm with $\tau_0 = 78$ ps. Then (A9) yields $A = 191$. The chief reason for the discrepancy in A (280 versus 191) is probably the uncertainty in P/A_{eff} in (A6).

E. Compressed Pulse Autocorrelations and Cross Correlations

Compressed pulse autocorrelations and cross correlations are illustrated in Figs. 5–7 and in [1], [3], and [4]. Use of the above-listed parameters in (2.7) gives $a_0 = 6.16$ ps^2 or $a_0/t_0^2 = 0.00315$.

In the calculations, the compressed pulse width and height are moderately sensitive to changes in the dimensionless quadratic phase coefficient a_0/t_0^2. Table II shows, for the two chirped pulse simulations described above, the values used in the present calculations and the value for maximum peak intensity I of the compressed pulse without any windowing.

ACKNOWLEDGMENT

We gratefully acknowledge stimulating discussions with P. F. Liao and P. W. Smith of Bell Communications Research, as well as with R. H. Stolen of AT&T Bell Laboratories who provided the optical fiber and information on its parameters.

REFERENCES

[1] J. P. Heritage, A. M. Weiner, and R. N. Thurston, "Picosecond pulse shaping by spectral phase and amplitude manipulation," *Opt. Lett.*, vol. 10, pp. 609–611, 1985. A different approach to Fourier pulse shaping, which uses nonchirped optical pulses, has been discussed by C. Froehly, B. Colombeau, and M. Vampouille, "Shaping and analysis of picosecond light pulses," in *Progress in Optics XX*, E. Wolf, Ed. Amsterdam: Holland, 1983, p. 115.

[2] W. J. Tomlinson, R. H. Stolen, and C. V. Shank, "Compression of optical pulses chirped by self-phase modulation in fibers," *J. Opt. Soc. Amer. B*, vol. 1, pp. 139–149, 1984.

[3] J. P. Heritage, R. N. Thurston, W. J. Tomlinson, A. M. Weiner, and R. H. Stolen, "Spectral windowing of frequency-modulated optical pulses in a grating compressor," *Appl. Phys. Lett.*, vol. 47, pp. 87–89, 1985.

[4] A. M. Weiner, J. P. Heritage, and R. N. Thurston, "Synthesis of phase coherent, picosecond optical square pulses," *Opt. Lett.*, vol. 11, pp. 153–155, 1986.

[5] J. Debois, F. Gires, and P. Tournois, "A new approach to picosecond laser pulse analysis shaping and coding," *IEEE J. Quantum Electron.*, vol. QE-9, pp. 213–218, 1973; J. Agostinelli, G. Harvey, T. Stone, and C. Gabel, "Optical pulse shaping with a grating pair," *Appl. Opt.*, vol. 18, pp. 2500–2504, 1979; A. M. Johnson, R. H. Stolen, and W. M. Simpson, "80× single-stage compression of frequency doubled Nd:yttrium aluminum garnet laser pulses," *Appl. Phys. Lett.*, vol. 44, pp. 729–731, 1984; A. M. Johnson, R. H. Stolen, and W. M. Simpson, "Generation of 0.41-picosecond pulses by single-stage compression of frequency doubled Nd:YAG laser pulses," in *Ultrafast Phenomena IV*, D. H. Auston and K. Eisenthal, Eds. New York: Springer-Verlag, 1984, pp. 16–18.

[6] R. H. Stolen and C. Lin, "Self-phase-modulation in silica optical fibers," *Phys. Rev. A*, vol. 17, pp. 1448–1453, 1978.

[7] R. H. Stolen, "Nonlinear properties of optical fibers," in S. E. Miller and A. G. Chynoweth, *Optical Fiber Telecommunications*. New York: Academic, 1979.

[8] D. Grischkowsky and A. C. Balant, "Optical pulse compression based on enhanced frequency chirping," *Appl. Phys. Lett.*, vol. 41, pp. 1–3, 1982.

[9] W. J. Tomlinson, R. H. Stolen, and A. M. Johnson, "Optical wave breaking of pulses in nonlinear optical fibers," *Opt. Lett.*, vol. 10, pp. 457–459, 1985.

[10] E. B. Treacy, "Optical pulse compression with diffraction gratings," *IEEE J. Quantum Electron.*, vol. QE-5, pp. 454–458, 1969.

[11] O. A. Martinez, J. P. Gordon, and R. L. Fork, "Negative group velocity dispersion using refraction," *J. Opt. Soc. Amer. A*, vol. 1, pp. 1003–1006, 1984.

[12] Having separated out the carrier exp ($j\omega_0 t$), we henceforth deal only with envelope functions, and the Fourier transform variable is understood to be $\Omega \equiv (\omega - \omega_0)$.

[13] See, for example, H. A. Haus, *Waves and Fields in Optoelectronics*. Englewood Cliffs, NJ: Prentice-Hall, 1984.

[14] More precisely, $A_{00}(\Omega)$ is the Fourier transform of the lowest Hermite–Gaussian component of the beam (and $a_{00}(t)$ in (3.9) is its temporal profile) after the second pass through the grating pair under the assumptions that the spatial spreading is undone exactly by the second pass and that the grating phase shift can be taken as purely quadratic with the constant coefficient a_0. The summation in (3.2) implies different Fourier transforms and temporal profiles for the higher order Hermite–Gaussian components because their effective frequency filters involve convolution of the physical mask and input beam with different spatial profiles. Our further assumption that these higher order components are not important in the present experiments (in which there is spatial filtering by apertures in the output path) is justified by the agreement of the calculations with the experimental results. Strictly, $A_{00}(\Omega)$ *at the mask* has only half of the phase correction. The other half occurs during the backward pass through the grating pair. Our a_0 accounts for the entire correction.

[15] Our numerical calculations of $E(\Omega)$ from $\hat{E}_{clb}(t)$ and of $a_{00}(t)$ from $A_{00}(\Omega)$ employ a standard fast Fourier transform (FFT) routine. See, for example, E. O. Brigham, *The Fast Fourier Transform*. Englewood Cliffs, NJ: Prentice-Hall, 1974.

[16] The half power position is the place where $S(\Omega) = (2)^{1/2}/2$, i.e., where the error function in (4.2) has the value $1 - (2)^{1/2}$. The corresponding error function argument is about -0.38535. Hence, the half power position is shifted from the physical edge by an amount $\delta x = 0.38535 \times w_0/(2)^{1/2} \approx 0.2725\, w_0$ or roughly a quarter of the spot size.

[17] The odd pulse is closely related to the zero area pulse which has been produced by propagation through an atomic vapor. J. E. Rothenberg, D. Grischkowsky, and A. C. Balant, "Observation of the formation of the 0π pulse," *Phys. Rev. Lett.*, vol. 53, p. 552, 1984.

[18] See, for example, A. Papoulis, *The Fourier Integral and Its Applications*. New York: McGraw-Hill, 1962.

[19] In the described experiments, our shortest compressed pulses conform to $\Delta t \cdot \Delta f \approx 0.8$ rather than the indicated transform limit of $\Delta t \cdot \Delta f$

= 0.441. Use of this longer Δt would change (7.2) to $\Delta T/\Delta t = 0.67m$.

[20] J. D. Kafka, B. H. Kolner, T. Baer, and D. M. Bloom, "Compressions of pulses from a continuous-wave mode-locked Nd:YAG laser," *Opt. Lett.*, vol. 9, pp. 505–506, 1984.

Robert N. Thurston (A'55–M'60–SM'73) received the B.S.M.E. degree from Illinois Institute of Technology, Chicago, in 1945 and the M.S. and Ph.D. degree in physics from Ohio State University, Columbus, in 1948 and 1952.

At Bell Laboratories from 1952–83 and at Bell Communications Research since then, he has done research in mechanics, electromechanical interactions, liquid crystal displays, and optics. His principal research topics include optical pulse shaping, liquid crystal phenomena for display applications, guided waves, wave propagation in crystals, anharmonic effects, piezo-resistive strain gauges, ultrasonic delay lines, electromechanical transducers, and mechanical filters. At Bell Communications Research, he is a member of the Physics and Optical Science Research Division where he is engaged in studies of optical pulse shoping, optical waveguides, and other devices for possible application to optical communications. He is the author of about 80 technical publications in these fields, has been issued 10 patents, and is coeditor of the series of books, *Physical Acoustics*.

Dr. Thurston is a member of the American Physical Society, the Society for Natural Philosophy, the Society of Engineering Science, the Optical Society of America, and is a Fellow of the Acoustical Society of America. He has been Associate Editor and Patent Reviewer for the Acoustical Society, has served the IEEE Group on Sonics and Ultrasonics as Administrative Committee member, Program Chairman and Associate Editor, and now serves on the Board of Directors of the Society of Engineering Science.

Jonathan P. Heritage (S'74–M'75) received the B.S. degree in electrical engineering from the University of California, Berkeley, in 1967, the M.S. degree in physics from San Diego State University, San Diego, CA, in 1971, and the Ph.D. degree in electrical engineering from the University of California, Berkeley, in 1975.

From 1975 to 1976, he was with the Physics Department of the Technical University of Munich, West Germany, as a Postdoctoral Fellow of the Alexander von Humbouldt Stiftung, where his studies concentrated on picosecond lifetime measurements in organic compounds. In 1976 he joined the staff of Bell Laboratories, Holmdel, NJ, where he was a Member of Technical Staff. Since January 1, 1984, he has been with Bell Communications Research, Inc. where he joined the Physics and Optical Sciences Research Division. His research has led to contributions to the development of high-sensitivity spectroscopy using synchronized, tunable picosecond lasers, vibrational stimulated Raman spectroscopy of surface monolayers, and surface enhanced nonlinear optics. Subsequently, he has investigated rapid carrier recombination in compound and layered semiconductors and its importance to the problem of temperature sensitivity of threshold in quaternary semiconductor lasers. His recent work has focused on picosecond pulse compression and on a technique for synthesizing arbitrarily shaped picosecond and subpicosecond pulses using the fiber and grating pulse compressor. His present interests include ultrafast processes in multiquantum-well structures and compound semiconductors, picosecond spectroscopy with tailored pulse shapes, and infrared picosecond lasers.

Dr. Heritage is presently an associate editor of the IEEE JOURNAL OF QUANTUM ELECTRONICS. He is a member of the American Physical Society and the Optical Society of America.

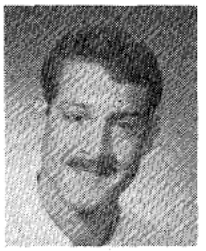

Andrew M. Weiner was born in Boston, MA, on July 25, 1958. He received the S.B., S.M., and Sc.D. degrees in electrical engineering from the Massachusetts Institute of Technology, Cambridge, in 1979, 1981, and 1984, respectively. From 1979 through 1984, he was a Fannie and John Hertz Foundation Graduate Fellow. His doctoral research included compression of femtosecond optical pulses and measurement of femtosecond dephasing times in condensed matter. For this research he received the 1984 Fannie and John Hertz Foundation Doctoral Thesis Prize.

Since 1984 he has been a member of the technical staff at Bell Communications Research in Holmdel, NJ. His research interests include generation and applications of picosecond and femtosecond pulses, pulse compression and pulse shaping, and measurement of picosecond electrical waveforms.

W. J. Tomlinson was born in Philadelphia, PA, on April 3, 1938. He received the S.B. and Ph.D. degrees in physics from the Massachusetts Institute of Technology, Cambridge, in 1960 and 1963, respectively.

After two years in the U.S. Army, he joined Bell Laboratories as a member of the Technical Staff in the research area, where he conducted research on gas lasers, organic photosensitive materials for data storage, holography recording and integrated optics, microoptical components for optical fiber systems, and nonlinear optics. From 1981 to 1983 he supervised an explanatory effort on optical recording. In 1983 he transferred to the newly-formed Bell Communications Research, as District Research Manager for Lightwave Component Technology Research. In his present position he is responsible for research on integrated optical components, and continues his research on nonlinear phenomena in optical fibers.